Classification of aerosols over Saudi Arabia from 2004–2016

Article (Accepted Version)

Classification of aerosols over Saudi Arabia from 2004−2016

Md. Arfan Ali[1, †], Janet E. Nichol[2, †], Muhammad Bilal[1*], Zhongfeng Qiu[1], Usman Mazhar[3], Md Wahiduzzaman[4], Mansour Almazroui[5], M. Nazrul Islam[5]

[1]School of Marine Sciences, Nanjing University of Information Science and Technology, Nanjing 210044, China

[2]Department of Geography, School of Global Studies, University of Sussex, UK

[3]School of Remote Sensing and Geomatics Engineering, Nanjing University of Information Science and Technology, Nanjing 210044, China

[4]Institute for Climate and Application Research, Nanjing University of Information Science and Technology, Nanjing 210044, China.

[5]Center of Excellence for Climate Change Research/Department of Meteorology, King Abdulaziz University, Jeddah 21589, Saudi Arabia

[*]Email: muhammad.bilal@connect.polyu.hk

†Authors with equal contributions.

Abstract

Knowledge of aerosol size and composition is very important for investigating the radiative forcing impacts of aerosols, distinguishing aerosol sources, and identifying harmful particulate types in air quality monitoring. The ability to identify aerosol type synoptically would greatly contribute to the knowledge of aerosol type distribution at both regional and global scales, especially where there are no data on chemical composition. In this study, aerosol classification techniques were based on aerosol optical properties from remotely-observed data from the Ozone Monitoring Instrument (OMI) and Aerosol Robotic Network (AERONET) over Saudi Arabia for the period 2004−2016 and validated using data from the Cloud-Aerosol Lidar and Infrared Pathfinder Satellite Observation (CALIPSO). For this purpose, the OMI-based Aerosol Absorption

Optical Depth (AAOD) and Ultra-Violet Aerosol Index (UVAI), and AERONET-based AAOD, Ångström Exponent (AE), Absorption Ångström Exponent (AAE), Fine Mode Fraction (FMF), and Single Scattering Albedo (SSA) were obtained. Spatial analysis of the satellite-based OMI-AAOD showed the dominance of absorbing aerosols over the study area, but with high seasonal variability. The study found significant underestimation by OMI AAOD suggesting that the OMAERUV product may need improvement over bright desert surfaces such as the study area. Aerosols were classified into (i) Dust, (ii) Black Carbon (BC), and (iii) Mixed (BC and Dust) based on the relationships technique, between the aerosol absorption properties (AAE, SSA, and UVAI) and size parameters (AE and FMF). Additionally, several of the parameter relationships misclassified the aerosol types over the study area, and only the FMF vs. AAE relationship was found to be robust. As expected, the dust aerosol type was dominant both annually and seasonally due to frequent dust storm events. Also, fine particulates such as BC and Mixed (BC and Dust) were observed, likely due to industrial activities (cement, petrochemical, fertilizer), water desalination plants, and electric energy generation. This is the first study to classify aerosol types over Saudi Arabia using several different aerosol property relationships, as well as over more than one site, and using data over a much longer time period than previous studies. aerosol relationship techniques such as FMF vs. UVAI etc. This enables classification and recognition of specific aerosol types over the Arabian Peninsula and similar desert regions.

Keywords: Aerosols; AERONET; Single Scattering Albedo; Absorption Ångström Exponent; Ozone Monitoring Instrument; Aerosol Absorption Optical Depth.

1 Introduction

Atmospheric aerosol particles comprise solid and liquid materials differing in size from a few nanometers to larger than 100 micro-meters, with intricate composition and volatility in their physiochemical properties (Almazroui, 2019). Over Asia, an immense diversity of aerosol types exist, due to rapid industrialization and urbanization. This creates uncertainty in assessing global climate change (Eck et al., 2010). Atmospheric aerosols are considered a major element of the earth's climate system, as they remodel the climate and radiative balance directly by scattering and absorbing incoming solar radiation (Ali et al., 2017), whilst indirectly changing cloud optical

properties and providing condensation nuclei (Kaufman et al., 2005). Classification of aerosols into different types can improve the precision of radiative balance, and assist climate modelling.

Aerosol types such as dust, organics, sea salt, and sulfate are predominantly reflective and scatter incoming solar radiation back to space, thus cooling the atmosphere (Bilal et al., 2013). However, other aerosols have more absorbing than scattering properties (Li et al., 2016). The main absorbers in the aerosol mixture are iron oxides from dust, and Black Carbon (BC) released from biomass burning and combustion processes and Brown Carbon (BrC) from organic mattter combustion (Wang et al., 2011). Moreover, iron oxides, BC and (BrC) show the greatest absorption from the ultraviolet (UV) to the visible region (Eck et al., 2010; Liakakou et al., 2020), while BC particles display constant absorption across the entire solar region (Bergstrom et al., 2002). A thorough understanding of climate forcing due to aerosol requires knowledge of aerosol concentration, its composition, size, and optical properties such as absorption or scattering. The aerosol size distribution and absorption properties can be used to classify the aerosols over the region (Higurashi and Nakajima, 2002; Lee et al., 2010). These properties vary spatially and temporally (Choi et al., 2009) according to the season, emission sources, and aerosol transportation (Ram et al., 2016).

The ground-based Aerosol Robotic Network (AERONET) provides aerosol absorptivity, from the Absorption Ångström Exponent (AAE) at 440–870 nm and Single Scattering Albedo (SSA) at 440 nm data. Complementing this, the Ozone Monitoring Instrument (OMI) on the Aura satellite also provides aerosol absorbing properties such as the Ultra-Violet Aerosol Index (UVAI) and Aerosol Absorption Optical Depth (AAOD) (Eq. 1) calculated in the UV and visible bands (Adesina et al., 2016) (Table 1). Light absorbing particles (e.g., dust, BC, or BrC) in the atmosphere can be determined by single scattering albedo (SSA) and absorbing aerosol optical depth (AAOD) (Shin et al., 2019). The AAOD is the columnar aerosol loading (i.e. AOD) due to light absorption based on the relationship

$$AAOD = (1\text{-}SSA) \times AOD \quad (1)$$

This is the most important parameter for the evaluation of atmospheric warming due to light absorbing aerosols. Hu et al. (2016) reported that high AAOD levels commonly found over East

Asia result mainly from aerosol mixtures comprising desert dust, industrial pollutants, and smoke from biomass burning. The study and classification of absorbing aerosols over the globe based on AERONET and satellite observations is well established (Cazorla et al., 2013; Logan et al., 2013; Logothetis et al., 2020; Kedia et al., 2014; Rupakheti et al., 2019, 2019a; Shen et al., 2019). Dubovik et al. (2002) established the relationship technique, which uses relationships between different optical properties of aerosols derived from AERONET and laboratory measurements, for the classification of global aerosols. Thus the relationship techniques of FMF (Fine Mode Fraction) vs. AE, FMF vs. AAE, FMF vs. SSA, AE vs. UVAI, and FMF vs. UVAI can be used to distinguish the major aerosol types (Tables 1 and 2). Since then, studies have r used different relationship techniques, including FMF vs. AE (Eck et al., 2010), FMF vs. AAE (Giles et al., 2011), FMF vs. SSA (Lee et al., 2010; Giles et al., 2012), AE vs. UVAI and FMF vs. UVAI (Bibi et al., 2017) to classify aerosols into dust modes and BC). For example, low values of FMF vs. AE indicate coarse mode dust aerosol (Aloysius et al., 2009); and high values of FMF (> 0.6) and intermediate values of AAE ($1.0 < AAE < 2.00$) indicate BC aerosols (Giles et al., 2011). Similarly, values of SSA ($SSA \leq 0.95$) and high values of FMF also indicate BC aerosols (Lee et al., 2010; Giles et al., 2012). Several studies have used relationship techniques from ground-based instruments alone, including Schmeisser et al. (2017), Jose et al. (2016) who classified absorbing aerosols over Hyderabad, India, Alam et al. (2016) over urban areas of Pakistan, and Gharibzadeh et al., (2018) over Iran.

However, only a few such studies are available over the Middle-East. . Of these, Farahat et al. (2016) reported only a single aerosol type: dust, over the Middle-East and North Africa. Al-Salihi (2018) classified aerosols based on single parameters and over only one site, Baghdad, Iraq, reporting four different aerosol types (maritime, dust, urban, and biomass burning). The few aerosol classification studies conducted over Saudi Arabia have used only one site in Saudi Arabia, the Solar Village, as part of larger studies in other regions. For example Logothetis et al. (2020) classified aerosols into eight types (Fine (highly, moderately, slightly, and non-absorbing), mixed (absorbing and non-absorbing), coarse (absorbing and non-absorbing)) based on FMF, SSA, and AE relationships over Europe, the Middle East, North-Africa and Arabian Peninsula. Kaskaoutis et al. (2007) classified aerosols into four types (clean maritime, biomass burning-urban, desert dust, and mixed) using relationship techniques over three continents and Other studies include

Chen et al. (2016) and Mao et al. (2019) who also included Saudi Arabia's Solar Village, Riyadh site as part of a larger study. None included the KAUST Campus site in Jeddah, which is situated at the other side of the country (Figure 1), and thus could offer a wider perspective of aerosol properties. Because Saudi Arabia has distinctive geographical and climatic environments, which differentiate it from other countries, accurate classification of aerosols cannot rely on universal classifications. High aerosol concentrations over Saudi Arabia have traditionally been attributed to frequent dust storms (Awad and Mashat, 2014; Almazroui et al., 2015; Awad et al., 2015; Kumar et al., 2018; Ali and Assiri, 2019; Mashat et al., 2019, 2020). However, the booming oil, and gas industry generating unprecedented economic growth, have stimulated, rapid urbanization and industrial

Table 1 Definition of aerosol optical properties and relationship indicators

Index designation	Name	Indicator
AAOD	Aerosol Absorption Optical Depth	Columnar aerosol loading of light absorbing aerosols
AE	Ångström Exponent	Indicates the size of the dominant aerosol particles in the column (AE < 1 specifies dominance of coarse mode and AE > 1 demonstrates the dominance of fine mode aerosol)
AAE	Absorption Ångström Exponent	Measures the spectral dependence of absorption (UV to NIR), which depends on size, shape, and chemical composition of aerosols. Dust and BC (absorbing aerosols) have high values > 2.
FMF	Fine Mode Fraction	Provides quantitative information about the proportion of coarse and fine mode aerosol particles. FMF < 0.40 = coarse mode, 0.4 ≤ FMF ≥ 0.6 = mixture, FMF > 0.60 = fine mode
SSA	Single Scattering Albedo	The ratio of scattering to extinction, and indicates the proportion of absorbing versus scattering aerosol particles SSA > 0.95 = non-absorbing, SSA ≤ 0.95 = absorbing aerosols
UVAI	Ultra-Violet Aerosol Index	A robust index for detecting absorbing aerosols (dust and soot) in the atmosphere. Uses 2 UV wavebands. UVAI > 1.0 = the enhanced presence of UV-absorbing, UVAI = 0.5-1.0 = weak presence of UV-absorbing aerosols.
FMF vs. AE	Low values of both = Dust, Medium values = Mixed (BC and Dust), High values = BC	
FMF vs. AAE	High values of AAE and low values of FMF indicate Dust, Medium values of both indicate Mixed (BC and Dust), Low values of AAE and High values of FMF indicate BC	
FMF vs. SSA	Low values of FMF and Medium values of SSA indicate Dust, Medium values of FMF and Low SSA indicate Mixed (BC and Dust), High values of both indicate BC.	
FMF vs. UVAI	Low values of FMF and High values of UVAI indicate Dust, Medium FMF and Low UVAI indicate Mixed (BC and Dust), High values of FMF and Low values of UVAI indicate BC	
AE vs. UVAI	Low values of AE and High values of UVAI indicate Dust, Medium AE, and Low UVAI indicate Mixed (BC and Dust), High values of AE, and Low values of UVAI indicate BC.	

activities (i.e., cement, petrochemical, fertilizer, water desalination, and electric energy generation plants). The outcomes are unquantified in terms of human health, as it is known that different aerosol types vary in their health impacts. Several studies have reported health impacts from heavy metals and pathogens accompanying dust storms over the Middle-East. For example, Leili et al. (2008) examined total suspended particles and PM_{10} over the centre of Tehran (Iran), and reported

heavy metal contents (Pb, Co, Cd, Cu, and Cr) at levels dangerous enough to cause neurodevelopmental and behavioral defects in children. Other findings of high heavy metal content of airborne dust in the Middle East include Foroushani et al. (2019) in western Iran, and Farahmandkia et al. (2010) in Tehran. Studies which linked heavy metals in dust with serious human health concerns include Leili et al (2008) in Tehran, Jiries et al. (2003) in Amman, Jordan, and Al-Rajhi et al. (1996) in Riyadh. In addition to heavy metals, Gerivani et al. (2011) found that dust storms in Iran can contain and transport viruses which affect human populations and Saeedi et al (2012) reported dust particles containing polycyclic aromatic hydrocarbons (PAHs) in Teheran. . A potentially beneficial impact of dust particles, is their role in carrying nutrients to the marine ecosystem of the Northern Red Sea (Jeddah) and their contribution to nutrient balance continues largely unexplored (Prakash et al., 2015). The amplified threats of climate change for desert animals world-wide are magnified in Saudi Arabia (Williams et al., 2012). Thus, the classification of aerosols over the Arabian Peninsula for accurate estimates of climate forcing and health impacts is urgent. This study uses available ground-based AERONET sites within Saudi Arabia i.e., the Solar Village and KAUST Campus sites, combined with satellite data from the Ozone Monitoring Instrument (OMI) to classify the predominant types of aerosols over Saudi Arabia.

The main highlights of the current research are (a) the long-term period of observations that makes the results more robust and (b) the selection based on comparison with CALIPSO of the most appropriate technique (classification scheme) for the determination of different aerosol types over Arabia.

2 Study area and Data-sets

2.1 Study Area

Saudi Arabia is the largest country in the Middle-East, covering 80% of the Arabian Peninsula with an area of approximately 2,218,000 km^2 (Figure 1), and is bordered by the Arabian Gulf and the Red Sea. The largest desert, the Rub al Khali or Empty Quarter covers 647,500 Km^2 in the southern part of the country and is a source of frequent dust outbreaks and severe dust storms. The country comprises 13 provinces and a total of 104 cities, of which the 20 largest have over 100,000 residents. This study was accomplished over the two AERONET ground stations in Saudi Arabia: Solar Village and KAUST Campus (Figure 1). The Solar Village (24.91˚ N, 46.41˚ E and

764 m a.s.l) is approximately 50 km from the north-west periphery of Riyadh. This city is situated on the desert plateau resulting in frequent dust storm events (Farahat, 2016). The KAUST Campus site (22.30˚ N, 39.10˚ E and 11.2 m a.s.l) is positioned in the village of Thuwal in a rural and coastal site in the Red Sea on the roof of a building. Climatically, the country has fairly wet autumn, winter and early spring seasons, and hot and dry late spring and summer seasons. Shamal winds lead to the increase of dust events during spring (Mashat et al., 2020) and summer (Notaro et al., 2013, 2015; Yu et al., 2013, 2015, 2016). Consequently, abundant aerosols were loaded during the spring and summer seasons over the KAUST Campus and Solar Village sites compared to the other seasons (Figure 1).

Based on the three-month mean readings of temperature and rainfall, Saudi Arabia's seasons are classified into spring from March to May (MAM), summer from June to August (JJA), autumn from September to November (SON), and winter from December to February (DJF) (AMS, 2001).

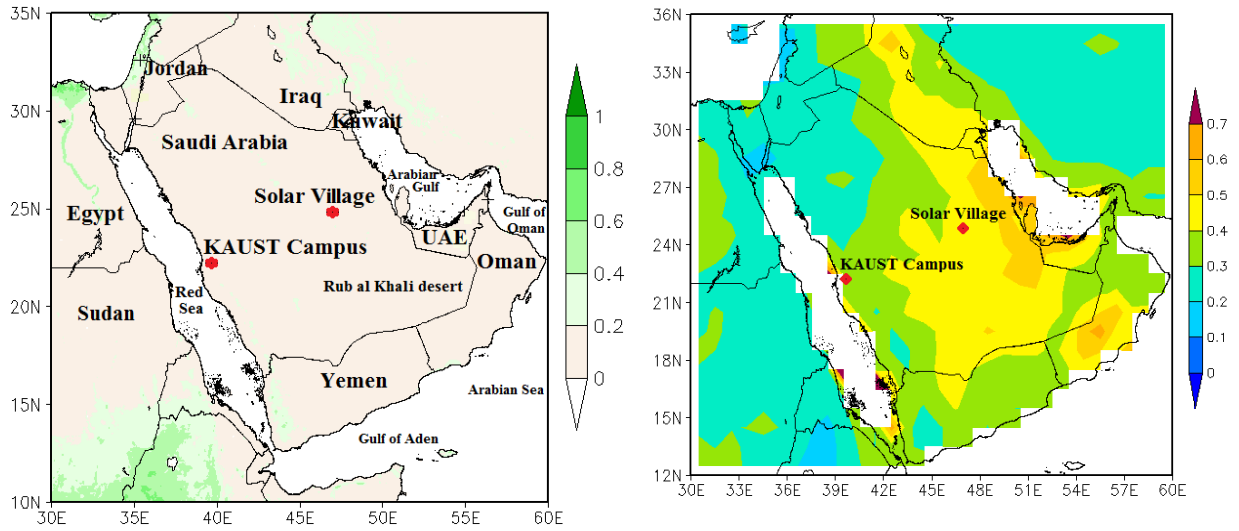

Figure 1: Geographical map of the Kingdom of Saudi Arabia. Red asterisks represent the two ground-based AERONET stations. Whereas, the left panel represents the mean values (2004–2016) of Normalized Difference Vegetation Index (NDVI) and the right panel represents the long term (2004–2016) mean values of aerosol optical depth (AOD) based on the MODIS Collection 6.1 Deep Blue algorithm.

2.2 Data-sets

OMI is carried by the Aura satellite, launched in July 2004, and is designed to measure air quality, the earth's climate, and ozone. It measures sunlight scattered by aerosols with high spectral resolution from the ultraviolet to visible regions (270−500 nm) and a spatial resolution of 13−24 km (Levelt et al., 2006). The OMI near-UV aerosol retrieval algorithm (OMAERUV) can be used to measure prominent absorbing aerosols such as dust and carbonaceous aerosols (Torres et al., 2007). The OMAERUV algorithm utilizes the near-UV spectral region for estimation of AAOD and UVAI products. Of major interest in the near-UV measurements is the powerful interaction between aerosol absorption and scattering in this spectral region, which facilitates the calculation of aerosol absorption capacity. For this study, OMI Level 2 and Level 3 OMAERUV OMI AAOD (500 nm) data were obtained from "https://giovanni.gsfc.nasa.gov/mapss/" and "https://giovanni.gsfc.nasa.gov/giovanni/", respectively.

The Cloud-Aerosol Lidar and Infrared Pathfinder Satellite Observation (CALIPSO) was launched on 28th April 2006 on the CloudSat satellite to study the roles of aerosols and clouds in earth's air quality, weather and climate. The CALIPSO gives information on aerosol vertical profiles and 3-dimensional information of aerosol properties throughout day and night over the globe (Winker et al., 2003), based on the Cloud-Aerosol Lidar with Orthogonal Polarization (CALIOP) sensor. The aerosol lidar ratio, a key parameter for extinction retrieval, is determined for each aerosol subtype based on measurements, modelling, and the cluster analysis of a multiyear Aerosol Robotic Network (AERONET) dataset (Omar et al., 2005, 2009), they are considered more accurate than other measurements. In version 3 (V3) and earlier, the CALIOP level 2 aerosol classification and lidar ratio selection algorithm defined six aerosol types: clean marine, dust, polluted continental, clean continental, polluted dust, and smoke (Omar et al., 2009). Each type is assigned an extinction-to-backscatter ratio (i.e., lidar ratio) with an associated uncertainty that defines the limits of its expected natural variability. (https://www.atmos-meas-tech.net/11/6107/2018/amt-11-6107-2018.pdf). This study used the Level 2 CALIPSO version 4.10 aerosol-type profiles for aerosol classification. These images were downloaded from https://www-calipso.larc.nasa.gov/products/lidar/browse_images/std_v4_index.php. The temporal resolution of 16 days for CALIPSO makes it unsuitable for continuous monitoring, but due to its accuracy, it is used in this study for validation.

The AERONET is NASA's ground-based aerosol network, which has more than 700 stations over the globe (Holben et al., 1998). The data are commonly used for validating satellite-based aerosol retrievals. In this study, version-3 Level 2.0 (cloud-screened and quality-assured) daily averaged direct sun products (FMF_{440nm} and $AE_{440\text{-}870nm}$) and sky irradiance products ($AAOD_{440nm}$, SSA_{440nm}, and $AAE_{440\text{-}870nm}$) were obtained from https://aeronet.gsfc.nasa.gov/ for the period 2004–2016 (Table 2).

Table 2 Observation and the total number of datasets at each AERONET site

Location	Observation	Total	
		Direct products AE/FMF	Inversion products SSA/AAE/AAOD
Solar Village	2004−May 2013	2463/2549	1001
KAUST Campus	Feb 2012−2016	1580/1393	1285

2.3 Research Methodology

The methodology of the present study is as follows: Mean seasonal and annual spatial distributions of OMI-AAOD were calculated from daily observations for the period 2004−2016. AERONET AAOD at 440 nm was interpolated to AAOD at 500 nm using the Ångström Exponent (Equation 1):

$$\mathrm{AAOD}_{500\ \mathrm{nm}} = \mathrm{AAOD}_{440\ \mathrm{nm}} \times \left(\frac{500}{440}\right)^{-\mathrm{AAE}_{440-870}} \quad (2)$$

Monthly and seasonal temporal analyses were performed for the AERONET data (AAOD, AE, AAE, FMF, and SSA) and OMI data (AAOD and UVAI). For validation purposes, to obtain collocated OMI-AAOD with AERONET, the OMI AAOD values were averaged for a spatial window of 1×1 pixel centered over the Solar Village and KAUST Campus sites, and AERONET values were averaged for +/- 30mins of the overpass time of OMI. Similarly, OMI UVAI collocated retrievals were obtained which were used for the classification of aerosol types. In the present study, a total of five relationships such as FMF vs. AE (Logothetis et al., 2020), FMF vs. SSA (Logothetis et al., 2020; Lee et al., 2010); AE vs. UVAI and FMF vs. UVAI (Bibi et al., 2017) were used. Besides, the FMF vs. AAE relationship is modified based on several previously published studies (Lee et al., 2010; Bibi et al., 2017; Rupakheti et al., 2019; Logothetis et al., 2020). The above relationships classified aerosols into three main categories (Table 3), namely (1)

dust, (2) mixed dust and black carbon (BC), and (3) BC (nearly exclusively attributed to fossil-fuel emissions, industrial and traffic). The remaining data points, which do not fall within the classification thresholds are denoted as other aerosol types. Finally, aerosol types were confirmed by comparison with satellite aerosol products from CALIPSO datasets.

Table 3 Classification of aerosol types over Saudi Arabia using threshold values taken from previous studies.

Aerosol Types	FMF vs AE		FMF vs AAE		FMF vs SSA	
Dust	FMF<0.4	AE<0.6	FMF<0.4	AAE>2.0	FMF<0.4	SSA≤0.95
Mixed (BC & Dust)	0.4≤FMF≤0.6	0.6≤AE≤1.2	0.4≤FMF≤0.6	1.0<AAE<2.0	0.4≤FMF≤0.6	SSA≤0.95
BC	FMF>0.6	AE> 1.2	FMF>0.6	1.0<AAE<2.0	FMF>0.6	SSA≤0.95
	AE vs UVAI				FMF vs UVAI	
Dust	0.0<AE<0.4	UVAI>1.57			0.1<FMF<0.3	UVAI>1.57
Mixed (BC & Dust)	0.0<AE<1.0	0.5<UVAI<1.55			0.1<FMF<0.55	0.5<UVAI<1.55
BC	1.0<AE>1.55	0.5<UVAI<1.52			0.55<FMF>1.0	0.5<UVAI<1.50

3 Results and discussion

3.1 Spatial distribution of OMI-based AAOD

Figures 2 and 3 show the mean annual and seasonal Level-3 OMI-AAOD retrievals at 500 nm of over Saudi Arabia for 2004−2016. Figure 2 shows high AAOD values (greater than 0.03) over the Eastern and Southern provinces, moderate AAOD (0.018 to 0.03) apparent over most parts of the country except the North-Western regions show low AAOD (0.01 to 0.018). These AAOD values are less than 10% of the columnar AOD values, which suggested that the absorbing aerosols are much less than scattering ones over Saudi Arabia. High AAOD is mainly distributed near dust, BC, and OC sources (Kang et al., 2017). Moreover, seasonal distributions (Figure 3) show the highest AAOD (greater than 0.03) in spring, and over the Eastern and Southern provinces, followed by summer, winter, and autumn. The reason for high AAOD during spring is the peak dust storm happens in this season when dust storms are originated or transported from the Sahara Desert by depressions passing eastwards over the Mediterranean Sea, the strong ground solar heating produces turbulence, local pressure gradients, and shamal pattern (Shao, 2008; Prakash et al., 2015; Mashat et al., 2019). The month of April to May (spring) is characterized by peak dustiness over Eastern and May-June over the Southern and Central regions of Saudi Arabia (Yu et al., 2013). Sabbah and Hasan (2008) also reported that spring is accounted for as a peak dust-aerosol season over Central Saudi Arabia. Moreover, dust-related aerosols are abundant over the Eastern parts of Saudi Arabia throughout the spring and summer (Prospero et al., 2002;

Washington et al., 2003; Goudie and Middleton, 2006; Ali et al., 2017). A high level of aerosols is reported over the Eastern province (Dhahran) due to the frequent sand and dust storms with industrial activities (Alharbi et al., 2013). In addition, the increased AAOD in winter may also reflect an enhanced presence of absorbing aerosols (BC, biofuel burning) during wintertime. The anticyclonic pattern is developed in autumn leading to weak dust activity resulting lowest columnar AAOD over Saudi Arabia (Kang et al., 2017; Mashat et al., 2019).

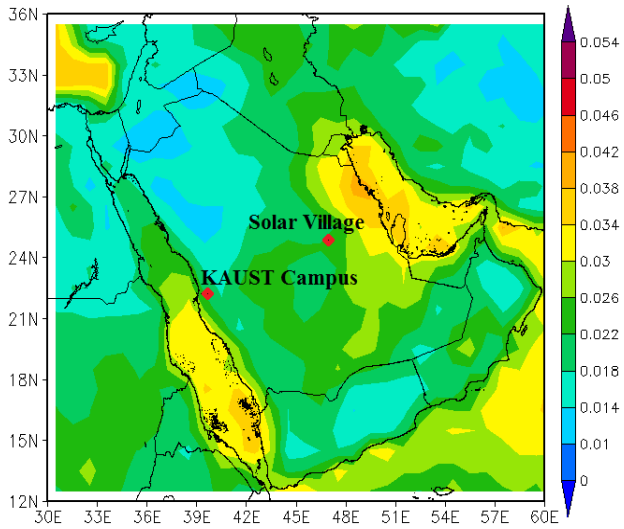

Figure 2: Annual mean Aerosol Absorption Optical Depth (AAOD) obtained from the OMI instrument over Saudi Arabia averaged over the period 2004−2016.

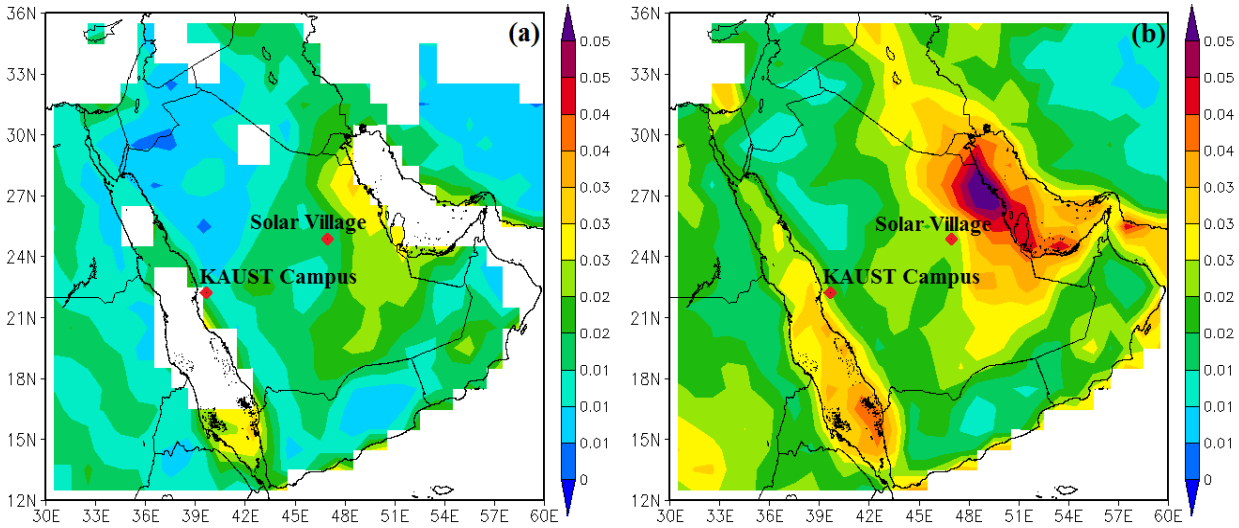

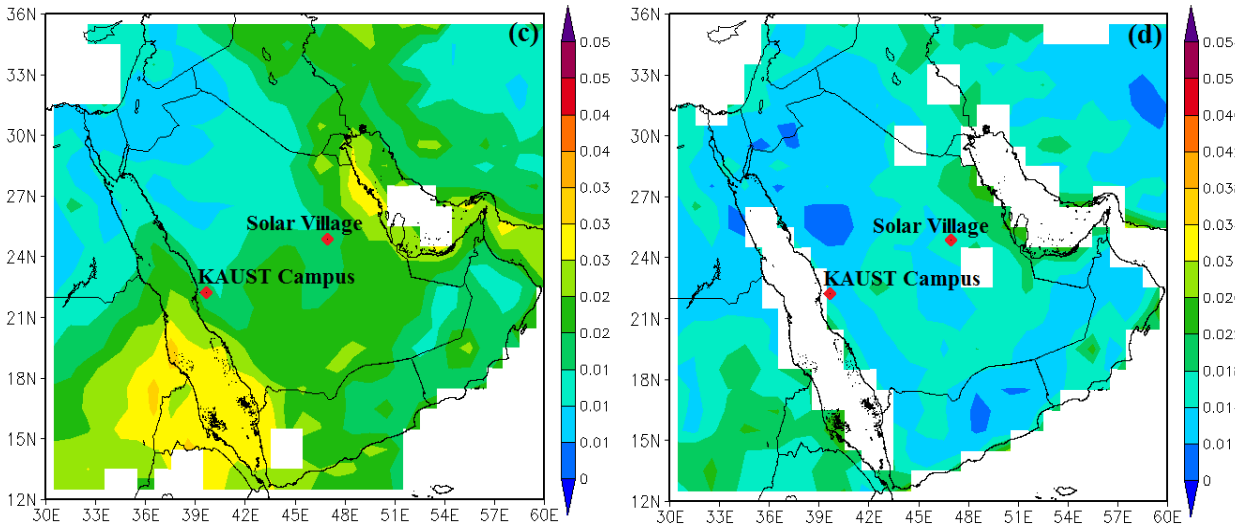

Figure 3: Mean seasonal spatial distribution of Aerosol Absorption Optical Depth (AAOD) for (a) Winter, (b) Spring, (c) Summer, and (d) Autumn obtained from OMI instrument over Saudi Arabia averaged over the period 2004−2016.

Figure 4 shows a more detailed annual cycle of both AERONET- and OMI-based Level-2 AAOD over the Solar Village (2004–2013) and KAUST Campus (2012–2016) sites. Higher values of AERONET and OMI AAOD retrievals over Solar Village in the east of the Peninsula, indicate more absorbing aerosols present than over the KAUST Campus site. The reason for high AAOD and more absorbing aerosols over Solar village may be due to a large number of dust storm events compared to the KAUST region as calculated using ground-based Meteorological station data (Butt et al., 2017). Results showed that OMI-AAOD retrievals followed the same temporal pattern as the AERONET-AAOD measurements but significant underestimation was observed in OMI-AAOD. Important to note that a large number of dust storm events lead to high dust-related aerosols which may be responsible for OMI (OMAERUV) underestimations in the Solar Village compared to the KAUST region. This may suggest that improvements in the OMI algorithm (OMAERUV) are required for a better estimation of AAOD over bright desert surfaces.

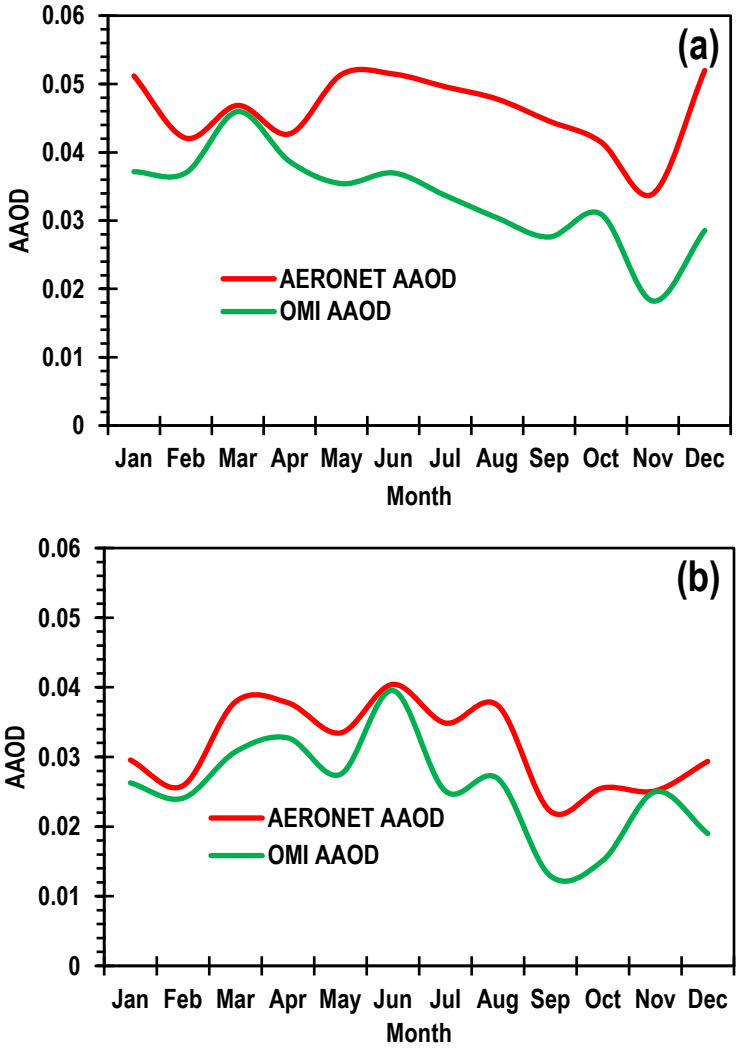

Figure 4: Annual cycle of Aerosol Absorption Optical Depth (AAOD) obtained from AERONET and Level 2 OMI instrument over the (a) Solar Village (2004−2013) and (b) KAUST Campus (2012−2016).

Figure 4 represents the annual cycle of AERONET- and OMI-based aerosol optical properties over the Solar Village and KAUST Campus sites for the period 2004−2016. These properties describe both aerosol size and absorptivity, including Ångström Exponent (AE), Absorption Ångström Exponent (AAE), Fine Mode Fraction (FMF), Single Scattering Albedo (SSA), and Aerosol Index (UVAI). The AE indicates the size of the dominant aerosol particles in the column, where small values of AE (< 1) indicate the dominance of coarse mode aerosols and large values of AE (> 1) demonstrate the dominance of fine mode aerosol such as BC, sulfate, and organic carbon released from man-made activities (Eck et al., 1999). The annual values of AE

(Table 4) suggest coarse mode aerosols over both AERONET sites (Solar Village: 0.48, KAUST Campus: 0.64), as well as in all seasons. AE reaches its minimum in May (Solar Village: 0.20, KAUST Campus: 0.35) and maximum in November (Solar Village: 0.86, KAUST Campus: 0.97) (Figure 5). These results suggest substantially more coarse mode aerosols in spring compared with other seasons. Trend analysis showed no significant increasing or decreasing trends in AE over either site (Table 4).

The Absorption Ångström Exponent (AAE) indicates the absorption contrast in relation to wavelength, which depends on particle size, shape, and chemical composition of the absorbing aerosols, which have a unique value (Russel et al., 2010; Li et al., 2016). For example, values of AAE < 2 and AAE > 2 indicate the fine mode and coarse mode absorbing aerosols respectively. Annual average values of AAE suggest coarse mode absorbing aerosols over both AERONET sites (Solar Village: 2.19, KAUST Campus: 2.27) (Table 4). However, significant variations were observed at monthly scales, with coarse mode absorbing aerosols observed in spring, but fine mode absorbing aerosols in winter over both sites (Figure 5). Overall, no significant decreasing/increasing trends in AAE were observed over either site (Table 4).

The Fine Mode Fraction (FMF) provides quantitative information about the proportion of coarse and fine mode aerosol particles, varying from 0 (coarse mode aerosols) to 1 (fine mode aerosols). According to Lee et al. (2010) and Logothetis et al. (2020), FMF < 0.40 represents coarse mode aerosols, 0.40 ≤ FMF ≤ 0.60 represents mixed type (coarse and fine mode) aerosols and FMF > 0.60 represents fine mode aerosols. The annual average value of FMF (0.34) in Solar Village is lower than that in KAUST Campus (0.40) and corresponds to more coarse mode aerosols over Solar Village. The seasonal average value of FMF (spring: 0.24, summer: 0.31, autumn: 0.44, winter: 0.38) in Solar Village is lower compared to FMF (spring: 0.30, summer: 0.37, autumn: 0.48, winter: 0.43) in KAUST Campus, which suggest more coarse-mode aerosols over Solar Village (Table 4). High levels of monthly mixed type aerosols were observed in November (0.52) followed by October and December (0.50), August (0.43) and January (0.42) in KAUST Campus compared to that in Solar Village (November: 0.52; December: 0.49, October: 0.44, and January:0.43), with the coarse mode at other times of year (Figure 5). Overall, no significant decreasing/increasing trends in FMF were observed over the years 2004−2016 (Table 4).

The Single Scattering Albedo (SSA) is the ratio of scattering to extinction and indicates the proportion of absorbing versus scattering aerosol particles. The value of SSA > 0.95 describes non-absorbing aerosols, $0.90 \leq SSA \leq 0.95$ indicates weakly absorbing aerosols, $0.85 < SSA < 0.90$ for moderately absorbing aerosols, and $SSA < 0.85$ belongs to highly absorbing aerosols (Lee et al., 2010; Russel et al., 2010; Gyawali et al., 2012; Shin et al., 2019). The annual average values of SSA within the range of 0.85−0.95 suggest the presence of weakly absorbing aerosols over both AERONET sites (Solar Village: 0.90, KAUST Campus: 0.93) (Table 4). At seasonal scale, weakly absorbing aerosols were observed during all seasons except during summer over the Solar Village site. Weakly absorbing aerosols indicate both dust and organic carbon, the latter being a complex mixture of chemical compounds generated from fossil fuel and biofuel burning as well as from natural biogenic emissions. The absorption or scattering property of dust grains depends on their size and composition, whether predominantly silicate or graphite, thus these results are compatible with the results of FMF and AE which suggest coarse aerosols to be dominant at both sites. Overall, no significant decreasing/increasing trends in SSA were observed (Table 4).

The Ultra-Violet Aerosol Index (UVAI) is a well-known index for detecting the absorbing aerosols (dust and bio-mass burning) in the atmosphere. It uses the UV spectrum to distinguish absorbing from non-absorbing aerosols (Graaf et al., 2005). The threshold UVAI > 0.5 is useful to identify absorbing aerosols (Torres et al., 2009). The value of UVAI > 1.0 shows the enhanced presence of UV-absorbing aerosols (e.g., dust or smoke or biomass burning), and $0.5 < UVAI < 1.0$ indicates the weak presence of UV-absorbing aerosols (Washington et al., 2003). The observed values of UVAI suggest the weak presence of UV-absorbing aerosols over both AERONET sites except spring in Solar Village and summer in KAUST Campus (Table 4). In contrast, the monthly observed values of UVAI suggest the enhanced presence of UV-absorbing aerosols in June followed by May and July over the KAUST Campus, while that in May followed by June and April over Solar Village (Figure 5). Kaskaoutis et al. (2010) also found the presence of dust particles as indicated by AI (0.5 to 0.6) over the South Greek. Overall, insignificant/significant increasing trends in UVAI were observed (Table 4).

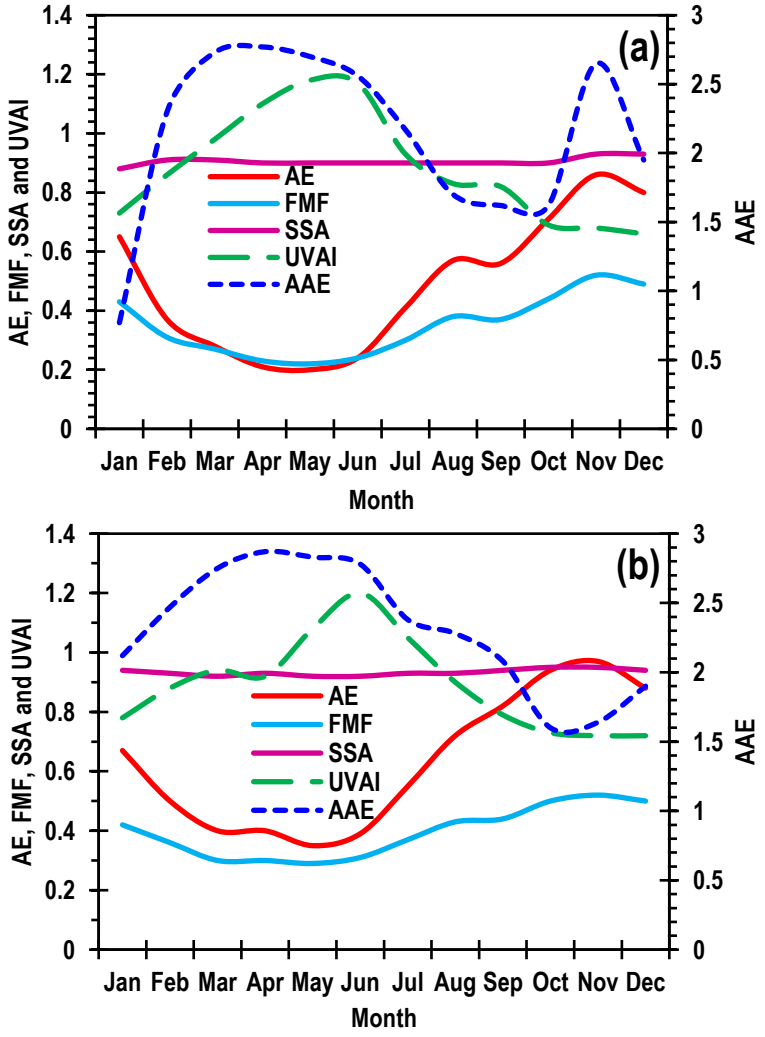

364 **Figure 5:** Annual cycle of averaged Aerosol Optical Properties obtained from AERONET (AE,
365 AAE, FMF, and SSA), and OMI (UVAI) over the (a) Solar Village site (2004−2013) and (b)
366 KAUST Campus site (2012−2016).

367

As can be seen from the above aerosol descriptions in this section 3.2, the analysis based on the individual parameters such as AE and FMF describe the mode, whether fine or coarse mode aerosols, AAE defines fine- and coarse- mode absorbing aerosols, both SSA and UVAI separates absorbing from non-absorbing aerosols. However, these individual parameters cannot identify the exact nature of the aerosol types such as dust or BC or mixed. Therefore section 3.3 evaluates the combination of these parameters to classify aerosols into specific types.

Table 4 Mean seasonal and annual variability of aerosol optical properties (AE, AAE, FMF, SSA, and UVAI) with their trends over the Solar Village and KAUST Campus sites for the period 2004−2016.

Parameters	Solar Village						KAUST Campus					
	Winter	Spring	Summer	Autumn	Annual	Trends	Winter	Spring	Summer	Autumn	Annual	Trends
AE	0.54±0.17	0.23±0.12	0.41±0.17	0.70±0.18	0.48±0.25	-0.012	0.68±0.20	0.39±0.08	0.55±0.17	0.91±0.12	0.64±0.24	0.023
AAE	2.14±0.93	2.72±0.36	2.18±0.70	1.70±0.66	2.19±0.71	-0.044	2.19±0.40	2.80±0.28	2.48±0.48	1.77 ± 0.47	2.27±0.57	0.067
FMF	0.38±0.08	0.24±0.07	0.31±0.08	0.44±0.08	0.34±0.11	-0.008	0.43±0.07	0.30±0.04	0.37±0.07	0.48±0.05	0.40±0.09	0.007
SSA	0.900±0.03	0.902±0.01	0.897±0.01	0.903±0.20	0.90±0.02	-0.001	0.94±0.01	0.92±0.01	0.93±0.01	0.95±0.01	0.93±0.01	0.002
UVAI	0.78±0.17	1.09±0.20	0.97±0.20	0.73±0.12	0.88±0.23	0.012	0.79±0.15	0.98±0.20	1.05±0.24	0.75±0.11	0.89±0.22	0.015*

3.3 Classification of aerosols

The relationships of different parameters such as FMF vs. AE, FMF vs. AAE, FMF vs. SSA, AE vs. UVAI, and FMF vs. UVAI were used to classify aerosols into three types such as Dust, Mixed (Dust and BC), and BC (Figure 6–9). Results based on FMF vs. AE, FMF vs. AAE, and FMF vs. SSA demonstrated the dominance of Dust type aerosols followed by Mixed (BC and Dust) and BC over the Solar Village and KAUST Campus sites except for AE vs. UVAI and FMF vs. UVAI relationships (Figures 6−7). According to the Figures (6 and 7 (a–c)), the relationship with higher percentages of the dominance of Dust type aerosols was noted from FMF vs. SSA (Solar Village: 84.04%, KAUST Campus: 50.50%) followed by FMF vs. AE (Solar Village: 63.88%, KAUST Campus: 48.38%), and

FMF vs. AAE (Solar Village: 58.10%, KAUST Campus:46.45%). Mostly lowest FMF values (<0.4) were noted over both sites due to the frequent dust storms (Kaskaoustis et al., 2007) and presented good relationships with low AE (<0.6), high AAE (AAE>2.0), and low SSA (≤ 0.95). A large number of frequent dust storms from the desert of Iraq, North-East of Saudi Arabia, and Southern Iran directly influence to the Solar Village site (Prospero et al., 2003; Farahat et al., 2016) resulting more dusty days were noticed over the Solar Village as compared to the KAUST Campus site (Yu et al., 2013; Butt et al., 2017). Therefore, dust aerosols are persistently prevalent over the Solar Village site. In contrast, the relationships of AE vs. UVAI and FMF vs. UVAI showed Mixed (BC and Dust) dominant aerosol type followed by Dust and BC (Figures 6 and 7 (d–e)). Since very low levels of dust aerosol type are indicated by the two relationships AE (Dust: 0.0<AE<0.4) vs. UVAI (Dust: >1.57) and FMF (Dust: 0.1<FMF<0.3) vs. UVAI (Dust: >1.57) over both sites, whereas other three relationships show high dust levels. Therefore, these results suggest that AE vs. UVAI and FMF vs. UVAI relationship cannot provide a meaningful aerosols type classification. This may be due to underestimation by the OMAERUV algorithm-based UVAI data, as the UVAI alone suggested the dominance of absorbing aerosols over both sites. Therefore, the study recommends that the OMAERUV algorithm needs improvement for better estimating the OMI UVAI over bright-reflecting surfaces.

Furthermore, it is important to note that the intermediate values of FMF ($0.4 \leq$ FMF ≤ 0.6) with intermediates values of AE ($0.6 \leq$ AE ≤ 1.2), AAE ($1.0 <$ AAE < 2.0), and SSA (≤ 0.95) represent coarse-mode dominated aerosols (Dust) which correspond to Mixed (Dust and BC) over the study area. It is evident from Figures 6 and 7 (a–c) that Mixed (Dust and BC) type aerosols were observed maximum from FMF vs. AE (Solar Village: 25.17%, KAUST Campus: 41.21%) followed by FMF vs. SSA (Solar Village: 13.49%, KAUST Campus: 28.51%) and FMF vs. AAE (Solar Village: 9.29%, KAUST Campus:19.18%). The value of FMF < 0.6 demonstrates coarse-mode dominated aerosols which were associated with a mixture of different types of aerosols (Wu et al., 2015). A similar finding was noted by Pérez-Ramírez et al., (2015) over Granada, Spain. Finally, Figures 6 and 7 (a–c) show small percentages of BC aerosols based on the above-mentioned three relationships over the both sites. Higher FMF (> 0.6) values indicate fine mode aerosols which correspond to BC which may be due to the local industrial activities (cement, petrochemical, fertilizer), water desalination plants, and electric energy generation (Farahat et al., 2016). Some aerosols datasets were not classified namely others aerosols found maximum over

the Solar Village site from FMF vs. AE (31.68%) than FMF vs. AE (8.43%) and FMF vs. SSA (0.51%), whereas, a large number of others aerosols were observed over the KAUST Campus site from FMF vs. AAE (29.97%) compared to FMF vs SSA (18.44%) and FMF vs. AE (6.75%) (Figures 6 and 7 (a–c). These aerosols might be formed due to the mixing of natural and anthropogenic aerosols with relative humidity over the study area (Kaskaoutis et al., 2011).

The seasonal distribution of aerosol types from the relationships FMF vs. AE, FMF vs. AAE, and FMF vs. SSA confirms the dominant Dust aerosols during all seasons over both sites, which reached its maximum in percentage during spring followed by summer, winter, and autumn (Figures 8 and 9 (a–c)). This confirms that the findings of previous satellite- and station-based studies which reported high dust levels during the peak dust storm season of spring and early summer (Sabbah and Hasan, 2008; Yu et al., 2013; Farahat et al., 2016; Albugami et al., 2019). Consequently, the lowest FMF values (< 0.3) were noted in spring and summer over both sites, which are associated with findings of Kaskaoutis et al. (2007) and Wu et al. (2015). Besides, the above-mentioned three relationships represent Mixed (Dust and BC) type aerosols during all seasons, which reach it's a peak in autumn followed by winter, summer, and spring over the study area (Figures 8 and 9 (a–c)). The possible reasons might be a sudden decrease in dust storm activities, due to all local anthropogenic activities (e.g., urban/industrial and biofuels emissions) and higher rainfall (Kaskoutais et al., 2007; Farahat et al., 2016), resulting FMF values become a little higher varies from 0.46 to 0.50 indicate coarse-mode dominated aerosols (Dust), which correspond to Mixed (Dust and BC) over the study area. The value of FMF < 0.6 demonstrates coarse-mode dominated aerosols which were associated with a mixture of different types of aerosols (Lee et al., 2010; Wu et al., 2015). Mostly BC aerosols were dominant during autumn and winter due to all local anthropogenic activities (e.g., urban/industrial and biofuels emissions). Consequently, the FMF values are boosted greater than 0.6 which were correlated with fine-mode BC particles over the study area. The findings of our study are supported by Gautam et al. (2007), Wu et al. (2015), and Lee et al. (2010).

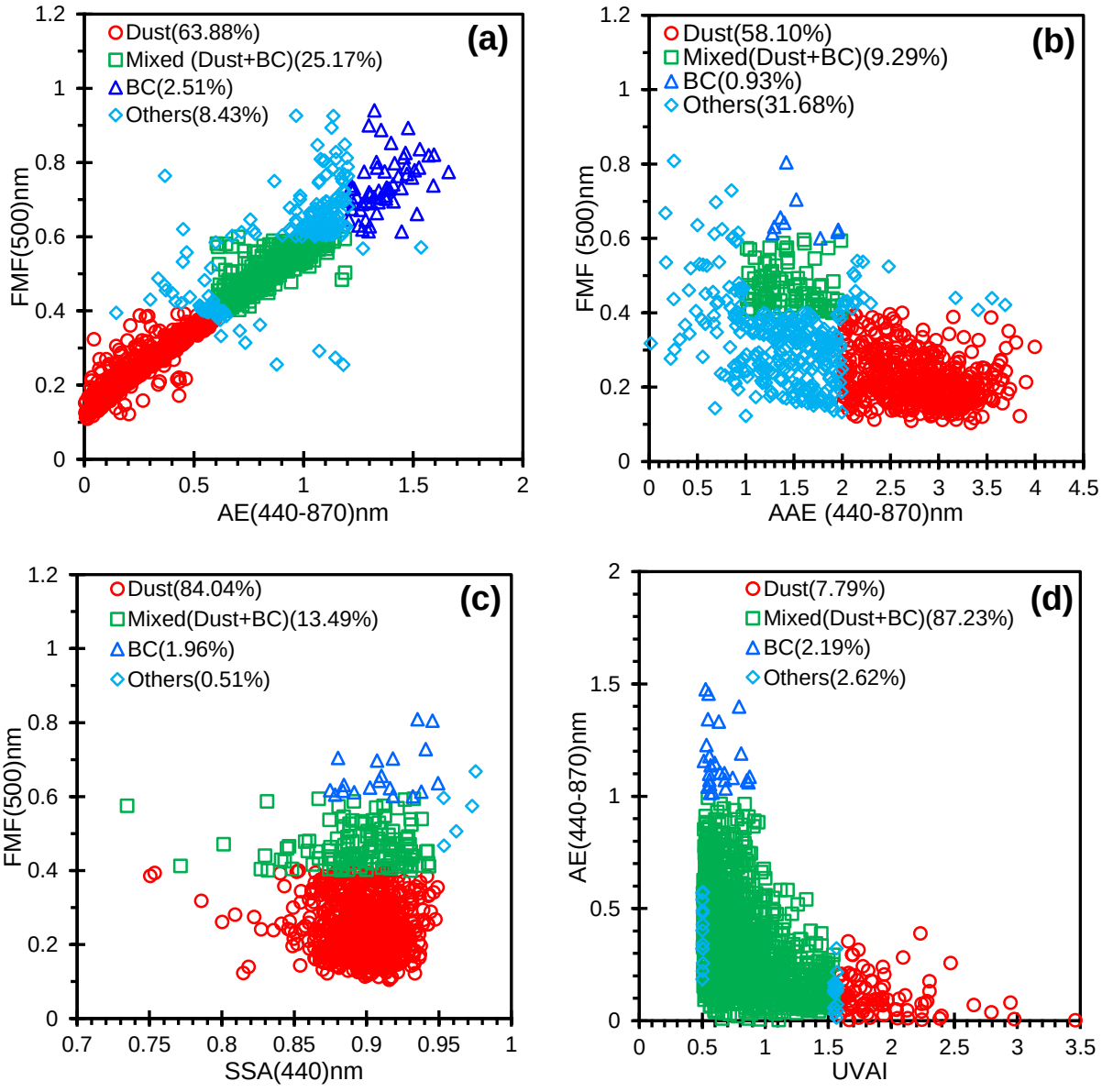
(a)
Dust(63.88%)
Mixed (Dust+BC)(25.17%)
BC(2.51%)
Others(8.43%)
FMF(500)nm
AE(440-870)nm
(b)
Dust(58.10%)
Mixed(Dust+BC)(9.29%)
BC(0.93%)
Others(31.68%)
FMF (500)nm
AAE (440-870)nm
(c)
Dust(84.04%)
Mixed(Dust+BC)(13.49%)
BC(1.96%)
Others(0.51%)
FMF(500)nm
SSA(440)nm
(d)
Dust(7.79%)
Mixed(Dust+BC)(87.23%)
BC(2.19%)
Others(2.62%)
AE(440-870)nm
UVAI

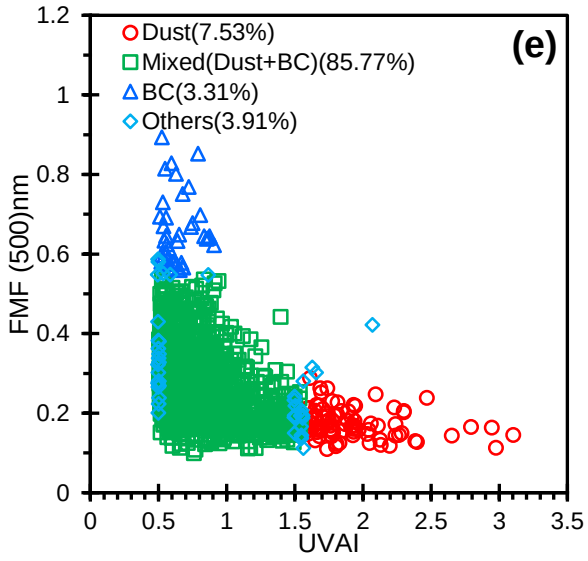

Figure 6: Aerosol classification over the Solar Village site during the period 2004-2013 for (a) FMF vs. AE, (b) FMF vs. AAE, (c) FMF vs. SSA, (d) AE vs. UVAI, and (e) FMF vs. UVAI.

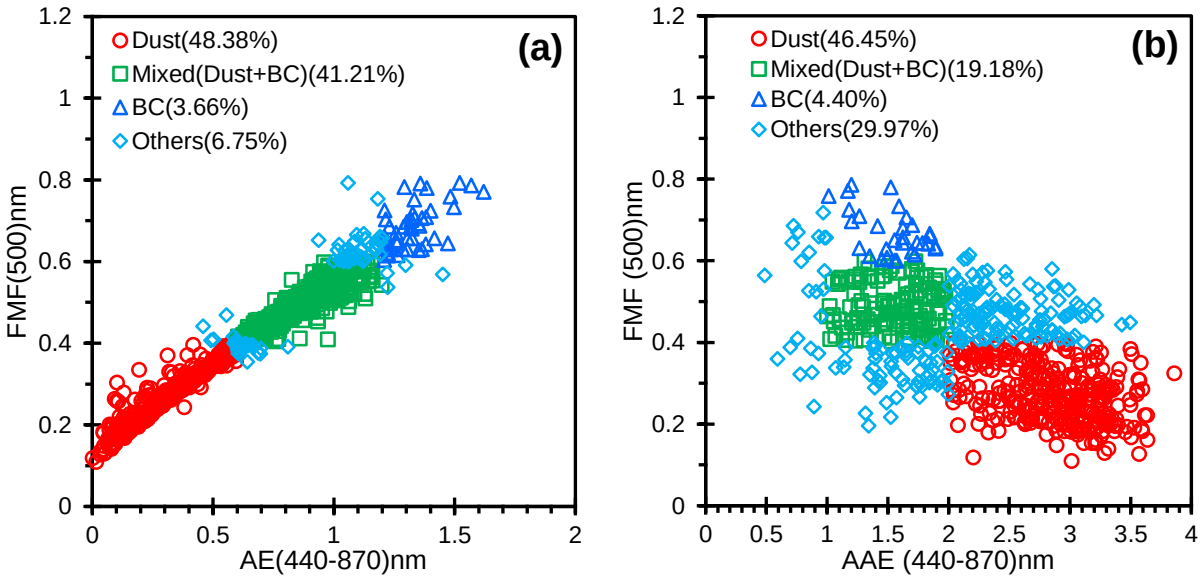

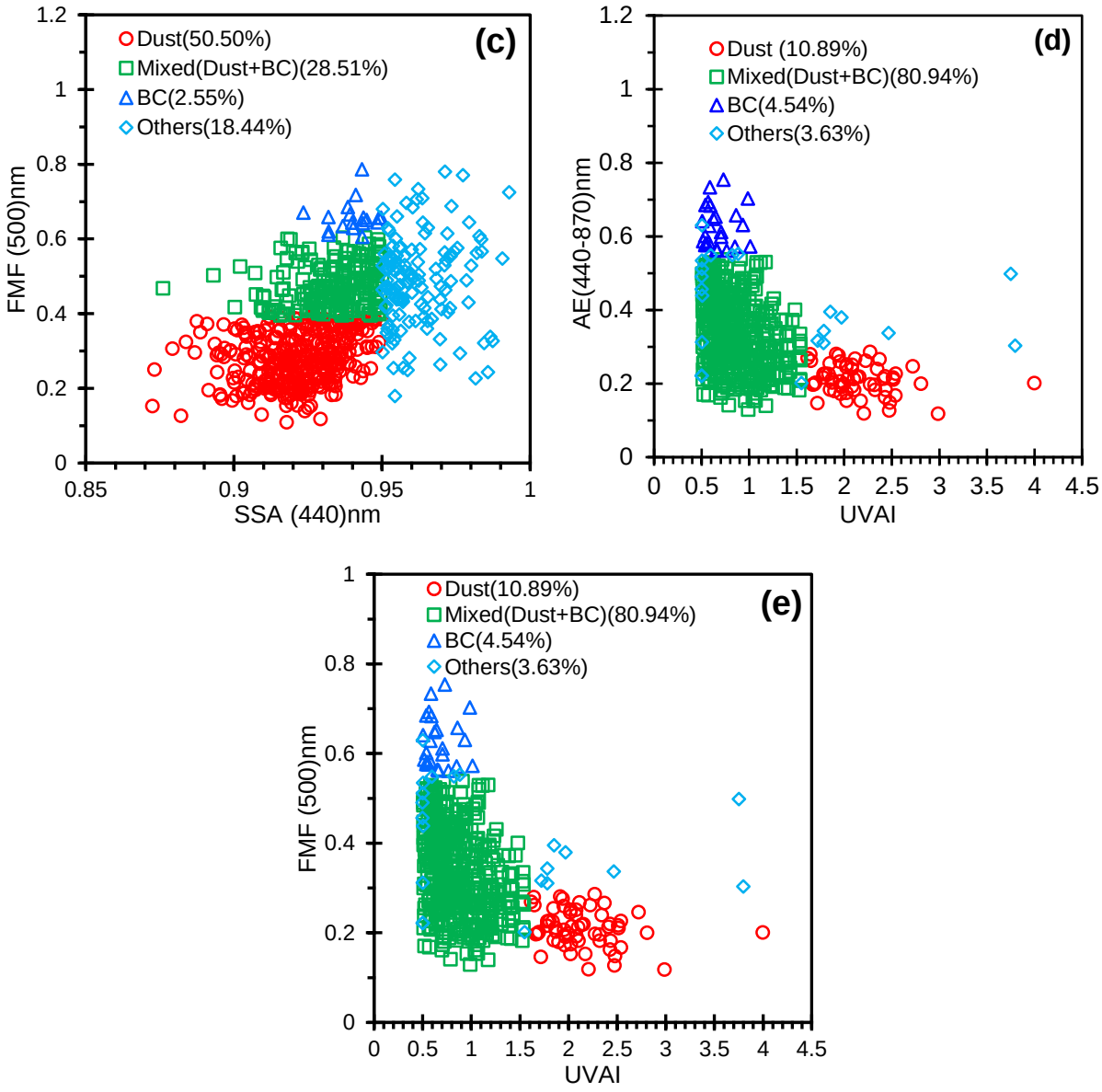

Figure 7: Aerosol classification over KAUST Campus site during the period 2012-2016 for (a) FMF vs. AE, (b) FMF vs. AAE, (c) FMF vs. SSA, (d) AE vs. UVAI, and (e) FMF vs. UVAI.

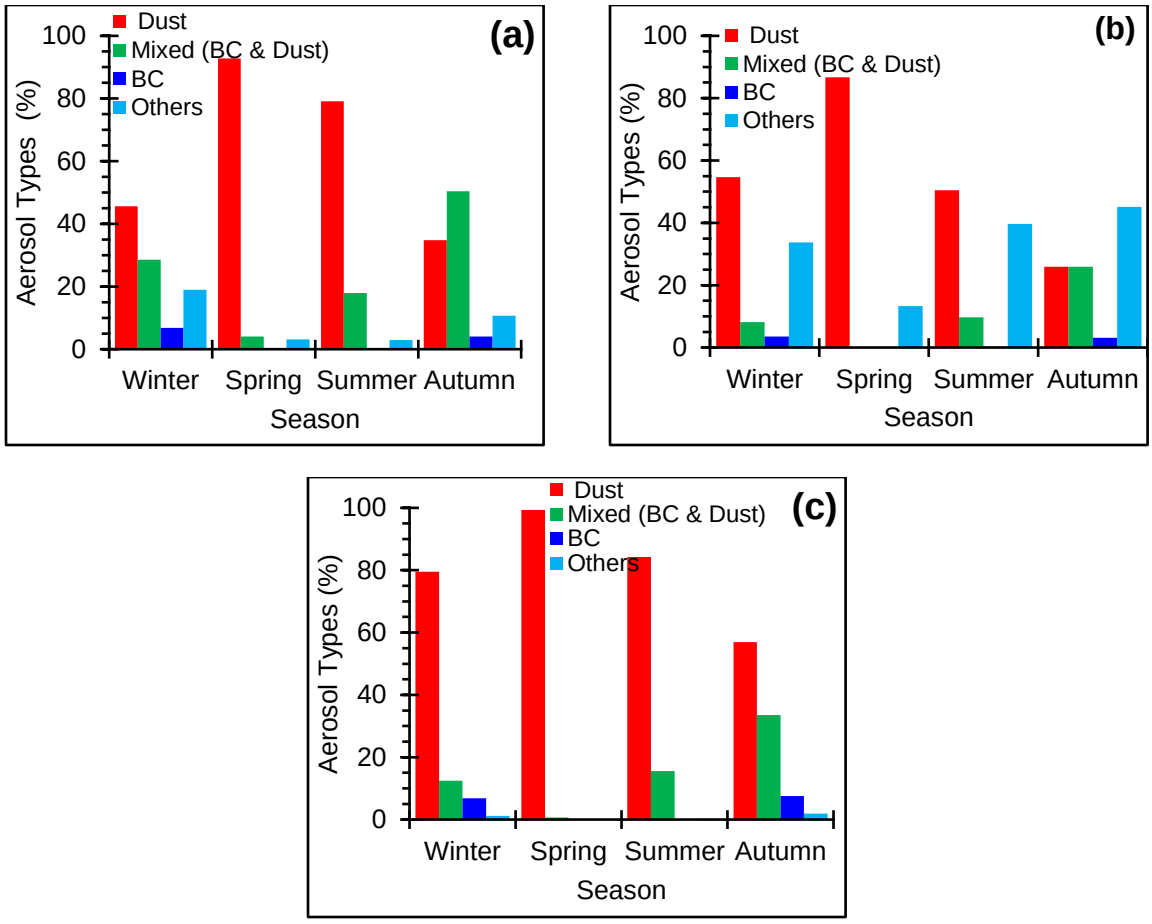

Figure 8: Seasonal aerosols classification over the Solar Village site during the period 2004-2013 for (a) FMF vs. AE, (b) FMF vs. AAE, (c) FMF vs. SSA.

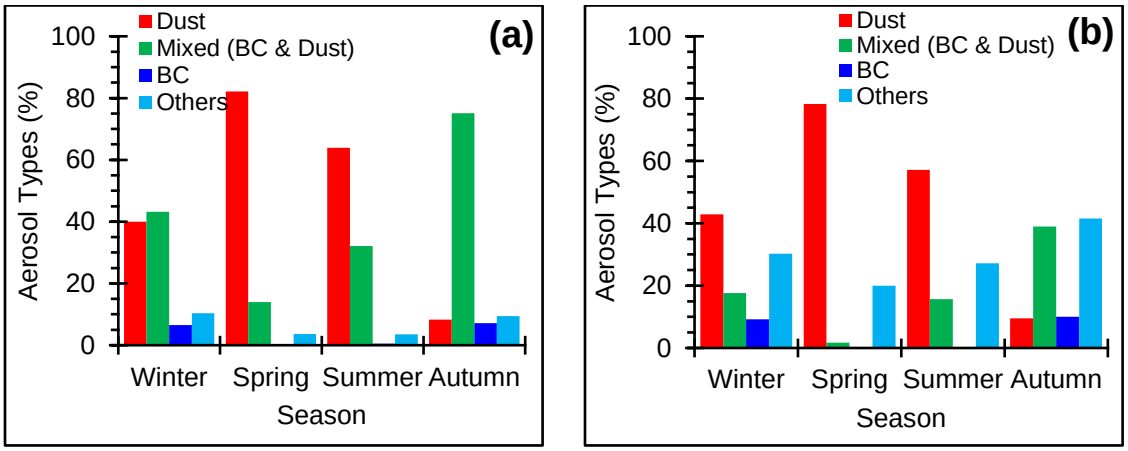

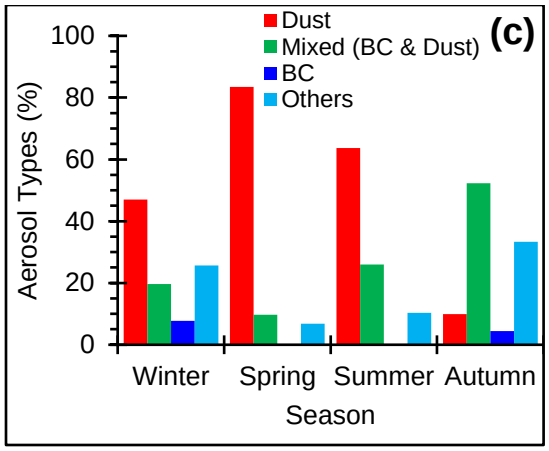

458

459 **Figure 9:** Seasonal aerosols classification over KAUST Campus site, Saudi Arabia during the
460 period 2012–2016 for (a) FMF vs. AE, (b) FMF vs. AAE, (c) FMF vs. SSA.

461

462 ***3.4 Validation of Classified Aerosol Types***

463 Classified aerosol types were validated against CALIPSO daytime aerosol type profiles.
464 Similar approach is also used by previous studies (Bibi et al., 2016, Bibi et al., 2017; Rupakheti et
465 al., 2019) as no other data are available for validation purpose. The CALIPSO (daytime) aerosol
466 type profiles were downloaded for specific dates, according to the availability of AERONET data,
467 including 24th Jul 2007, 11th Jul 2010, 06th Mar 2011, 29th Mar 2011, and 21st Apr 2008 for the
468 Solar Village site, and 23rd May 2012, 25th Jan 2013, 10th Feb 2013, 5th Mar 2013, and 02nd Jun
469 2013 for the KAUST Campus site. Results from CALIPSO showed the dominance of dust aerosols
470 reaching up to 5 km from the surface over both sites (Table 5 and Figure S1–S2). Results also
471 showed the presence of other mixed aerosols (i.e. dust plumes and biomass burning mixed, and
472 forming polluted dust) over the study area (Table 5 and Figure S1–S2). The results showed a good
473 agreement of FMF vs. AE, FMF vs. AAE, and FMF vs. SSA classified aerosol types with
474 CALIPSO-based aerosol types over the region. Therefore, this study recommends to use the above-
475 mentioned three techniques for aerosols classification over Saudi Arabia and other regions with
476 similar atmospheric and land surface characteristics.

477

478

479

480

481

Table 5 Aerosol classifications based on FMF vs. (AE, AAE, and SSA) and CALIPSO.

Date	FMF vs. AE		Types	FMF vs. AAE		Types	FMF vs. SSA		Types	CALIPSO
Site: Solar Village										
24-Jul-2007	0.24	0.26	Dust	0.24	2.43	Dust	0.24	0.89	Dust	Dust
21-Apr-2008	0.15	0.04	Dust	0.15	3.23	Dust	0.15	0.92	Dust	Dust
11-Jul-2010	0.32	0.46	Dust	0.32	2.70	Dust	0.32	0.93	Dust	Dust
06-Mar-2011	0.25	0.36	Dust	0.25	3.45	Dust	0.25	0.88	Dust	Dust
29-Mar-2011	0.13	0.01	Dust	0.13	2.92	Dust	0.13	0.92	Dust	Dust
Site: KAUST Campus										
23-May-2012	0.29	0.23	Dust	0.29	2.89	Dust	0.29	0.90	Dust	Dust
25-Jan-2013	0.48	0.91	Mixed	0.48	1.41	Mixed	0.48	0.93	Mixed	Mixed
10-Feb-2013	0.37	0.55	Dust	0.37	2.01	Dust	0.37	0.93	Dust	Dust
5-Mar-2013	0.37	0.56	Dust	0.37	2.49	Dust	0.37	0.94	Dust	Dust
02-Jun-2013	0.19	0.10	Dust	0.19	3.15	Dust	0.19	0.90	Dust	Dust

4. Conclusion

In this paper, aerosol types were classified using OMI ($AAOD_{500nm}$, UVAI) and AERONET ($AAOD_{440nm}$, $AE_{440\text{-}870nm}$, $AAE_{440\text{-}870nm}$, FMF_{440nm}, SSA_{440nm}) data over Saudi Arabia for the period 2004–2016. The main findings of the present studies are: (1) High AAOD values over the Eastern and Southern provinces and lower AAOD over the Northern province; (2) Significant underestimation in OMI-AAOD products compared to AERONET AAOD was observed, suggesting significant improvements required for OMI algorithm (OMAERUV) for better estimation of AAOD over bright desert surfaces; (3) Notable temporal variations in aerosols (i.e., coarse and fine mode particles) were observed based on the aerosol optical properties from AERONET (i.e., AE, AAE, FMF, and SSA) and OMI (UVAI); (4) This study found that the FMF vs. UVAI and AE vs. UVAI relationships misclassified aerosol types over the study area, therefore the FMS vs. AE, FMF vs. AAE, and FMF vs. SSA relationships are recommended for aerosol classification over Saudi Arabia and areas with similar land and atmospheric characteristics; (5) Aerosol classification showed dust to be the most common and abundant aerosol type at both annual and seasonal scales, and this was expected, due to the frequent dust storm activity over the study area; (6) The presence of BC and Mixed (Dust and BC) aerosols, though in lesser amounts than dust, which are attributed by increasing industrial activities (i.e., cement, petrochemical, fertilizer), water desalination plants, infrastructure, and electric energy demand. These release absorbing and fine particles, which often become mixed with dust; (7) Validation against CALIPSO data showing that aeorosl classifiation relationships such as FMF vs. AE, FMF vs.

AAE, and FMF vs. SSA are robust and effective to lassify aerosol over the region. In view of increased knowledge of the harmful health effects of dust-borne synthetic compounds, the aerosol classification techniques described here should be of great benefit in future air quality control programs.

Acknowledgment

The authors are grateful to the NASA Goddard Space Flight Center and Goddard Earth Sciences Data and Information Services Center (GESDISC) for providing OMI (UVAI and AAOD) and AERONET data. We would like to give special thanks to the scientific teams of CALIPSO for making the data available for this study. This research is supported by the Special Project of Jiangsu Distinguished Professor (1421061801003 and 1421061901001), the National Natural Science Foundation of China (Grant No. 41976165), and the Startup Foundation for Introduction Talent of NUIST (2017r107). The foremost author is highly grateful to the China Scholarship Council (CSC) and NUIST to grant the fellowship and providing the required supports.

References

Adesina, J.A., Kumar, K.R., Sivakumar, V., Piketh, S.J., 2016. Intercomparison and assessment of long-term (2004−2013) multiple satellite aerosol products over two contrasting sites in South Africa. J. Atmos. Sol. Terr. Phys. 148, 82−95.

Alam, K., Shaheen, K., Blaschke, T., Chishtie, F., Khan, H.U., Haq, B.S., 2016. Classification of Aerosols in an Urban Environment on the Basis of Optical Measurements. Aerosol and Air Quality Research, 16: 2535–2549.

Albugami, S., Palmer, S., Cinnamon, J., Meersmans, J., 2019. Spatial and Temporal Variations in the Incidence of Dust Storms in Saudi Arabia Revealed from In Situ Observations. Geosciences 9, 162; doi:10.3390/geosciences9040162.

Ali, M.A., Assiri, M.E., 2019. Analysis of AOD from MODIS- Merged DT–DB Products over the Arabian Peninsula. Earth Syst. Environ. 3, 625–636.

Ali, M.A., Assiri, M., Dambul, R., 2017. Seasonal Aerosol Optical Depth (AOD) variability using satellite data and its comparison over Saudi Arabia for the period 2002–2013. Aerosol Air Qual. Res. 17, 1267–1280.

534 Ali, M.A., Islam, M.M., Islam, M.N., Almazroui, M., 2019. Investigations of MODIS AOD and
535 cloud properties with CERES sensor based net cloud radiative effect and a NOAA
536 HYSPLIT Model over Bangladesh for the period 2001–2016. Atmos. Res. 215, 268−283.
537 Almazroui, M., 2019. A comparison study between AOD data from MODIS deep blue collections
538 51 and 06 and from AERONET over Saudi Arabia. Atmos. Res. 225, 88−95.
539 Almazroui, M., Dambul, R., Islam, M.N., Jones, P.D., 2015. Atmospheric circulation patterns in
540 the Arab region and its relationships with Saudi Arabian surface climate: a preliminary
541 assessment. Atmos. Res. 161–162, 36–51.
542 Aloysius, M., Mohan, M., Suresh Babu, S., Parameswaran, K., Moorthy, K.K., 2009. Validation
543 of MODIS derived aerosol optical depth and an investigation on aerosol transport over the
544 South East Arabian sea during ARMEX-II. Ann. Geophys. 27, 2285−2296.
545 AMS, 2001. Statement on seasonal to inter-annual climate prediction. Bull. Am. Meteorol. Soc.
546 82, 701–703.
547 Al-Rajhi, M.A., Seaward, M.R.D., Al-Aamer, A.S., 1996. Metal levels in indoor and outdoor dust
548 in Riyadh, Saudi Arabi. Environment International, 22, 315-324.
549 Al-Salihi, A.M., 2018. Characterization of aerosol type based on aerosol optical properties over
550 Baghdad, Iraq. Arab. J. Geosci. 11, 633.
551 Awad, A., Mashat, A., 2014. The synoptic patterns associated with spring widespread dusty days
552 in central and eastern Saudi Arabia. Atmosphere 5 (4), 889–913.
553 Awad, A.M., Mashat, A.S., Salem, F.F.A., 2015. Diagnostic study of spring dusty days over the
554 southwest region of the Kingdom of Saudi Arabia. Arab. J. Geosci. 8, 2265–2282.
555 Bergstrom, R.W., Russell, P.B., Hignett, P., 2002. Wavelength dependence of the absorption of
556 black carbon particles: predictions and results from the TARFOX experiment and
557 implications for the aerosol single scattering albedo. J. Atmos. Sci. 59, 567−577.
558 Bibi, H., Alam, K., Bibi, S., 2016. In-depth discrimination of aerosol types using multiple
559 clustering techniques over four locations in Indo-Gangetic plains. Atmos. Res. 181,
560 106−114.
561 Bibi, S., Alam, K., Chishtie, F., Bibi, H., 2017. Characterization of absorbing aerosol types using
562 ground and satellites based observations over an urban environment. Atmos. Environ. 150,
563 126−135.

564 Bilal, M., Nichol, J.E., Bleiweiss, M.P., Dubois, D.W. 2013. A Simplified high resolution MODIS
565 Aerosol Retrieval Algorithm (SARA) for use over mixed surfaces. Rem. Sens. Environ.
566 136, 135–145.
567 Cazorla, A., Bahadur, R., Suski, K., Cahill, J.F., Chand, D., Schmid, B., Ramanathan, V., Prather,
568 K., 2013. Relating aerosol absorption due to soot, organic carbon, and dust to emission
569 sources determined from in-situ chemical measurements. Atmos. Chem. Phys. 13,
570 9337−9350.
571 Chen, Q.X., Yuan, Y., Shuai, Y., Tan, H.P., 2016. Graphical aerosol classification method using
572 aerosol relative optical depth. Atmos. Environ. 135, 84–91.
573 Choi, Y.-S., Ho, C.-H., Oh, H.-R., Park, R.J., Song, C.-G., 2009. Estimating bulk optical properties
574 of aerosols over the western North Pacific by using MODIS and CERES measurements.
575 Atmos. Environ. 43, 5654−5660.
576 Dubovik, O., Holben, B.N., Eck, T.F., Smirnov, A., Kaufman,Y.J., King, M.D.,Tanre, D.,
577 Slutsker,I., 2002. Variability of absorption and optical properties of key aerosol types
578 observed in worldwide locations. J. Atmos. Sci. 59, 590–608.
579 Eck, T., Holben, B.N., Reid, J., Dubovik, O., Smirnov, A., O'Neill, N., Slutsker, I., Kinne, S.,
580 1999. Wavelength dependence of the opticaldepth of biomass burning, urban, and desert
581 dust aerosols. J. Geophys. Res. 104(D24), 31333– 31349.
582 Eck, T.F., Holben, B.N., Sinyuk, A., Pinker, R., Goloub, P., Chen, H., Chatenet, B., Li, Z., Singh,
583 R.P., Tripathi, S.N., 2010. Climatological aspects of the optical properties of fine/coarse
584 mode aerosol mixtures. J. Geophys. Res. 115, D19205.
585 Farahat, A., 2016. Air pollution in the Arabian Peninsula (Saudi Arabia, the United Arab Emirates,
586 Kuwait, Qatar, Bahrain, and Oman): Causes, effects, and aerosol categorization. Arab. J.
587 Geosci. 9, 196.
588 Farahat, A., El-Askary, H., Adetokunbo, P., Fuad, A.-T., 2016. Analysis of aerosol absorption
589 properties and transport over North Africa and the Middle East using AERONET data.
590 Ann. Geophys., 34, 1031–1044.
591 Farahmandkia, Z., Mehrasbi, M.R., Sekhavatjou, M.S., 2010. Relationship between concentrations
592 of heavy metals in wet precipitation and atmospheric PM10 particles in Zanjan, Iran.
593 Iranian Journal of Environmental Health and Sciences Engineering, 8, 49−56.

Foroushani, M.A., Opp, C., Groll, M., 2019. Chemical Characterization of Aeolian Dust Deposition in Southern and Western Iran. Asian J. Geograph. Res. 2,1−22.

Gautam, R., Hsu, N.C., Kafatos, M., Tsay, S.-C., 2007. Influences of winter haze on fog/low cloud over the Indo-Gangetic plains. J. Geophys. Res. 112, D05207, doi:10.1029/2005JD007036.

Gerivani, H., Lashkaripour, G.R., Ghafoori, M., Jalali, N., The source of dust storm in Iran: A case study based on geological information and rainfall data. Carpathian J. Earth Environ. Sci. 2011, 6.

Gharibzadeh, M., Alam, K., Abedini, Y., Bidokhti, A.A., Masoumi, A., Bibi, H., 2018. Characterization of aerosol optical properties using multiple clustering techniques over Zanjan, Iran, during 2010-2013. Appl Opt. 57:2881−2889.

Gyawali, M., Arnott, W.P., Zaveri, R.A., Song, C., Moosmüller, H., Liu, L., Mishchenko, M.I., Chen, L.-W.A., Green, M.C.,Watson, J.G., Chow, J.C., 2012. Photoacoustic optical propertiesat UV, VIS, and near IR wavelengths for laboratory generatedand winter time ambient urban aerosols. Atmos. Chem. Phys. 12, 2587–2601.

Giles, D.M., Holben, B.N., Eck, T.F., Sinyuk, A., Smirnov, A., Slutsker, I., Dickerson, R., Thompson, A., Schafer, J., 2012. An analysis of AERONET aerosol absorption properties and classifications representative of aerosol source regions. J. Geophys. Res. 117, D17203.

Giles, D.M., Holben, B.N., Tripathi, S.N., Eck, T.F., Newcomb, W.W., Slutsker, I., Dickerson, R.R., Thompson, A.M., Mattoo, S., Wang, S.H., 2011. Aerosol properties over the Indo-Gangetic Plain: a mesoscale perspective from the TIGERZ experiment. J. Geophys. Res. 116, D18203.

Goudie, A.S., 2014. Desert dust and human health disorders. Environment International 63, 101-113.

Graaf, D.M., Stammes, P., Torres, O., Koelemeijer, R., 2005. Absorbing aerosol index: sensitivity analysis, application to GOME and comparison with TOMS. J. Geophys. Res. 110, D01201.

Hermida, L., Merino, A., Sánchez, J.L., Fernández-González, S., García-Ortega, E., López, L., 2017. Characterization of synoptic patterns causing dust outbreaks that affect the Arabian Peninsula. Atmos. Res., 199, 29−39.

Higurashi, A., Nakajima, T., 2002. Detection of aerosol types over the East China Sea near Japan from four-channel satellite data. Geophys. Res. Lett. 29, 1836.

Holben, B.N., Eck, T., Slutsker, I., Tanre, D., Buis, J., Setzer, A., Vermote, E., Reagan, J.A., Kaufman, Y., Nakajima, T., 1998. AERONETda federated instrument network and data archive for aerosol characterization. Rem. Sens. Environ. 66, 1−16.

Hu, Z., Zhao, C., Huang, J., Leung Ruby, L., Qian, Y., Yu, H., Huang, L., Kalashnikova, O., 2016. Trans-Pacific transport and evolution of aerosols: Evaluation of quasi-global WRF-Chem simulation with multiple observations. Geosci. Model Dev. 9, 1725–1746.

Hsu, N.C., Gautam, R., Sayer, A.M., Bettenhausen, C., Li, C., Jeong, M.J., Tsay, S.-C., Holben, B.N., 2012. Global and regional trends of aerosol optical depth over land and ocean using SeaWiFS measurements from 1997 to 2010. Atmos. Chem. Phys. 12, 8037–8053.

Jiries, A., 2003. Vehicular Contamination of Dust in Amman, Jordan. The Environmentalist 23, 205–210.

Jose, S., Niranjan, K., Gharai, B., Rao, P.V.N., Nair, V.S., 2016. Characterisation of absorbing aerosols using ground and satellite data at an urban location, Hyderabad. Aeros. Air Qual. Res. 16, 1427−1440.

Kang, J. Liu, T., Keller, J., Lin, H., 2013. Asian dust storm events are associated with an acute increase in stroke hospitalisation. J. Edipemiol. Community Health 67, 125−131.

Kang, L., Chen, S., Huang, J., Zhao, S., Ma, X., Yuan, T., Zhang, X., Xie, T., 2017. The Spatial and Temporal Distributions of Absorbing Aerosols over East Asia. Remote Sens. 9, 1050; doi:10.3390/rs9101050.

Kaskaoutis, D.G., Kambezidis, H.D., Hatzianastassiou, N., Kosmopoulos, P.G., Badarinath, K.V.S., 2007. Aerosol Climatology: On the discrimination of aerosol types over four AERONET sites. Atmos. Chem. Phys. Discuss. 7, 6357−6411.

Kaskaoutis, D.G., Kumar Kharol, S., Sinha, P.R., Singh, R.P., Kambezidis, H.D., Rani Sharma, A., Badarinath, K.V.S., 2011. Extremely large anthropogenic aerosol component over the Bay of Bengal during winter season. Atmos. Chem. Phys. 11, 7097−7117.

Kaskaoutis, D.G., Nastos, P.T., Kosmopoulos, P.G., Kambezidis, H.D., Kharol, S.K., Badarinath, K.V.S., 2010. The Aura-OMI Aerosol Index distribution over Greece. Atmos. Res, 98, 28-39.

Kaufman, Y., Boucher, O., Tanre, D., Chin, M., Remer, L., Takemura, T., 2005. Aerosol anthropogenic component estimated from satellite data. Geophys. Res. Lett. 32, L17804. http://dx.doi.org/10.1029/2005GL023125.

Kedia, S., Ramachandran, S., Holben, B.N., Tripathi, S., 2014. Quantification of aerosol type, and sources of aerosols over the Indo-Gangetic Plain. Atmos. Environ. 98, 607−619.

Khaniabadi, Y.O., Daryanoosh, S.M., Amrane, A., Polosa, R., Hopke, P.K. et al.. 2017. Impact of Middle Eastern Dust storms on human health. Atmos. Poll. Res. 8, 606−613.

Kim, D., Chin, M., Bian, H., Tan, Q., Brown, M.E., Zheng, T., You, R., Diehl, T., Ginoux, P., Kucsera, T., 2013. The effect of the dynamic surface bareness on dust source function, emission, and distribution, J. Geophys. Res. 118, 1–16.

Kumar, K.R., Attada, R., Dasari, H.P., Vellore, R.K., Langdon, S., Abualnaja,Y.O., Hoteit, I., 2018. Aerosol Optical Depth variability over the Arabian Peninsula as inferred from satellite measurements. Atmos. Environ. 187, 346−357.

Lee, K., Chung, C., 2012. Observationally-constrained estimates of global small mode AOD. Atmos. Chem. Phys. Discuss. 12, 31663−31698.

Lee, J., Kim, J., Song, C., Kim, S., Chun, Y., Sohn, B., Holben, B.N., 2010. Characteristics of aerosol types from AERONET sunphotometer measurements. Atmos. Environ. 44, 3110−3117.

Leili, M., Naddafi, K., Nabizadeh, R., Yunesian, M., Mesdaghinia, A., 2008. The study of TSP and PM10 concentration and their heavy metal content in central area of Tehran, Iran. Air Qual Atmos Health 1, 159–166.

Levelt, P.F., Hilsenrath, E., Leppelmeier, G.W., van den Oord, G.H., Bhartia, P.K., Tamminen, J., de Haan, J.F., Veefkind, J.P., 2006. Science objectives of the ozone monitoring instrument. IEEE Geosci. Remote Sens. Lett. 44, 1199−1208.

Li, J., Liu, C., Yin, Y., Kumar, K.R., 2016. Numerical investigationon the Ångström Exponent of black carbon aerosols. J. Geophys.Res. 121, 3506–3518.

Logan, T., Xi, B., Dong, X., Li, Z., Cribb, M., 2013. Classification and investigation of Asian aerosol absorptive properties. Atmos. Chem. Phys. 13, 2253−2265.

Logothetis, S.-A., Salamalikis, V., Kazantzidis, A., 2020. Aerosol classification in Europe, Middle East, North Africa and Arabian Peninsula based on AERONET Version 3. Atmos. Res., 239, 104893.

Mashat, A.W.S., Awad, A.M., Alamoudi, A.M., Assiri, M.E., 2019. Monthly and seasonal variability of dust events over northern Saudi Arabia. Int. J. Climatol. 2019, 1–23.

Mashat, A.W.S., Awad, A.M., Assiri, M.E., Labban, A.H., 2020. Dynamic and synoptic study of spring dust storms over northern Saudi Arabia. Theor. Appl. Climatol. 140, 619–634.

Omar, A.H., Won, J.-G., Winker, D.M., Yoon, S.-C., Dubovik, O., McCormick, M.P., 2005. Development of global aerosol models using cluster analysis of Aerosol Robotic Network (AERONET) measurements. J. Geophys. Res., 110, D10S14.

Omar, A.H., Winker, D.M., Vaughan, M.A., Hu, Y., Trepte, C.R., Ferrare, R.A., Lee, K.P., Hostetler, C.A., Kittaka, C., Rogers, R.R., Kuehn, R.E., 2009. The CALIPSO Automated Aerosol Classification and Lidar Ratio Selection Algorithm. J. Atmos. Ocean. Tech. 26, 1994–2014.

Onishi, K. Otani, S., Yoshida, A., Mu, H., Kurozawa, Y., 2012. Adverse Health Effects of Asian Dust Particles and Heavy Metals in Japan. Asia-Pacific Journal of Public Health Asia Pac J Public Health 27, NP1719-26.

Pérez-Ramírez, D., Veselovskii, I., Whiteman, D.N., Suvorina, A., Korenskiy, M., et al., 2015. High temporal resolution estimates of columnar aerosol microphysical parameters from spectrum of aerosol optical depth by linear estimation: application to long-term AERONET and star-photometry measurements. Atmos. Meas. Tech. 8, 3117–3133.

Prakash, P.J., Stenchikov, G., Kalenderski, S., Osipov, S., Bangalath, H., 2015. The impact of dust storms on the Arabian Peninsula and the Red Sea. Atmos. Chem. Phys. 15, 199–222.

Prospero, J.M., Ginoux, P., Torres, O., Nicholson, S.E., Thomas, E.G., 2002. Environmental characterization of global sources of atmospheric soil dust identified with Nimbus 7 total ozone mapping spectrometer (TOMS) absorbing aerosol product. Rev. Geophys. 40: 2–31.

Ram, K., Singh, S., Sarin, M., Srivastava, A., Tripathi, S., 2016. Variability in aerosol optical properties over an urban site, Kanpur, in the Indo-Gangetic Plain: a case study of haze and dust events. Atmos. Res. 174, 52−61.

Rupakheti, D., Kang, S., Bilal, M., Gong, J., Xia, X., Cong, Z., 2019. Aerosol optical depth climatology over Central Asian countries based on Aqua-MODIS Collection 6.1 data: Aerosol variations and sources. Atmos. Environ. 207, 205–214.

Rupakheti, D., Kang, S., Rupakheti, M., Cong, Z., Panday, A.K., Holben, B.N., 2019a. Identification of absorbing aerosol types at a site in the northern edge of Indo-Gangetic Plain and a polluted valley in the foothills of the central Himalayas. Atmos. Res. 223, 15-23.

Russell, P., Bergstrom, R., Shinozuka, Y., Clarke, A., DeCarlo, P., Jimenez, J.,Livingston, J., Redemann, J., Dubovik, O., Strawa, A., 2010. Absorption Ångström Exponent in AERONET and related data as an indicator of aerosol composition. Atmos. Chem. Phys. 10, 1155−1169.

Sabbah, I., Hasan, F.M., 2008. Remote sensing of aerosols over the Solar Village, Saudi Arabia. Atmos. Res. 90, 170–179.

Saeedi, M. Li, L.Y., Salmanzadeh, M., 2012. Heavy metals and polycyclic aromatic hydrocarbons: Pollution and ecological risk assessment in street dust of Tehran. Journal of Hazardous Materials 227–228, 9–17.

Schmeisser, L., Andrews, E., Ogren, J. A., Sheridan, P., Jefferson, A., et al., 2017. Classifying aerosol type using in situ surface spectral aerosol optical properties. Atmos. Chem. Phys. 17, 12097−12120.

Shao, Y., 2008. Physics and Modelling of Wind Erosion, Springer, Berlin, Germany.

Shen, X., Bilal, M., Qiu, Z., Sun, D., Wang, S., Zhu, W., 2019. Long-term spatiotemporal variations of aerosol optical depth over Yellow and Bohai Sea. Environ. Sci. Poll. Res. 26, 7969–7979.

Shin, S.K., Tesche, M., Noh, Y., Müller, D. 2019. Aerosol-type classification based on AERONET version 3 inversion products. Atmos. Meas. Tech., 12, 3789–3803.

Shin, S.K., Tesche, M., Müller, D., and Noh, Y. 2019. Technical note: Absorption aerosol optical depth components from AERONET observations of mixed dust plumes. Atmos. Meas. Tech., 12, 607–618.

Tiwari, S., Srivastava, A.K., Singh, A.K., Singh, S., 2015. Identification of aerosol types over Indo-Gangetic Basin: implications to optical properties and associated radiative forcing. Environ. Sci. Poll. Res. 22, 12246–12260.

Torres, O., Chen, Z., Ahn, C., 2009. Aerosol absorption measurements from space by the Aura-OMI sensor. In: Proc. STAR Science Seminar, NOAA-NESDIS, Camp Springs, MD. https://www.star.nesdis.noaa.gov/star/documents/seminardocs/Torres_20090702.pdf.

Torres, O., Tanskanen, A., Veihelmann, B., Ahn, C., Braak, R., Bhartia, P.K., Veefkind, P., Levelt, P., 2007. Aerosols and surface UV products from Ozone Monitoring Instrument observations: an overview. J. Geophys. Res. 112, D24S47.

747 Wang, S., Fang, L., Gu, X., Yu, T., Gao, J., 2011. Comparison of aerosol optical properties from
748 Beijing and Kanpur. Atmos. Environ. 45, 7406−7414.
749 Washington, R., Todd, M., Middleton, N.J., Goudie, A.S., 2003. Dust storm source areas
750 determined by the Total Ozone Monitoring Spectrometer and surface observations. Ann.
751 Assoc. Amer. Geogr. 93, 297–313.
752 Wilks, D.S., 2006. Statistical Methods in the AtmosphericSciences, Academic Press, Amsterdam
753 Boston, Heidelberg, London.
754 Williams, J.B., Shobrak, M., Wilms, T.M., Arif, I.A., Khan, H.A., 2012. Climate change and
755 animals in Saudi Arabia. Saudi Journal of Biological Sciences 19, 121–130.
756 Winker, D.M., Pelon, J.R., McCormick, M.P., 2003. The CALIPSO mission: spaceborne lidar for
757 observation of aerosols and clouds. In: Third International Asia-Pacific Environmental
758 Remote Sensing of the Atmosphere, Ocean, Environment, and Space. International Society
759 for Optics and Photonics,pp. 1e11. Proc. SPIE 4893.
760 Wu, Y.L., Li, H.W., Chien, C.H., Lai, Y.C., Wang, L.C., 2010. Monitoring and Identification of
761 Polychlorinated Dibenzo-p-dioxins and Dibenzofurans in the Ambient Central Taiwan.
762 Aeros. Air Qual. Res. 10, 463–471.
763 Wu, Y., Zhu, J., Che, H., Xia, X., Zhang, R., 2015. Column-integrated aerosol optical properties
764 and direct radiative forcing based on sun photometer measurements at a semi-arid rural site
765 in Northeast China. Atmos. Res. 157, 56–65.
766 Yu, Y., M. Notaro, Z. Liu, O. Kalashnikova, F. Alkolibi, E. Fadda, and F. Bakhrjy (2013),
767 Assessing temporal and spatial variations in atmospheric dust over Saudi Arabia through
768 satellite, radiometric, and station data. J. Geophys. Res. Atmos. 118, 13253–13264.
769